ACS APPLIED MATERIALS & INTERFACES

Research Article

www.acsami.org

Unraveling the Degradation Process of $LiNi_{0.8}Co_{0.15}Al_{0.05}O_2$ Electrodes in Commercial Lithium Ion Batteries by Electronic Structure Investigations

Karin Kleiner,[*,†,§] Julia Melke,[†,∥] Michael Merz,[‡] Peter Jakes,[⊥] Peter Nagel,[‡] Stefan Schuppler,[‡] Verena Liebau,[§] and Helmut Ehrenberg[†]

[†]Institute for Applied Materials−Energy Storage Systems, and [‡]Institute of Solid State Physics, Karlsruhe Institute of Technology, 76344 Eggenstein-Leopoldshafen, Germany

[§]BMW Group, 80788 Munich, Germany

[∥]Physical and Theoretical Chemistry, Freie Universitaet Berlin, Takustrasse 3, D-14195 Berlin, Germany

[⊥]Institute of Energy and Climate Research, Forschungszentrum Juelich, 52425 Juelich, Germany

Supporting Information

ABSTRACT: The degradation of $LiNi_{0.8}Co_{0.15}Al_{0.05}O_2$ (LNCAO) is reflected by the electrochemical performance in the fatigued state and correlated with the redox behavior of these cathodes. The detailed electrochemical performance of these samples is investigated by galvanostatic and voltammetric cycling as well as with the galvanostatic intermittent titration technique (GITT). Near-edge X-ray absorption fine structure (NEXAFS) spectroscopy was used to investigate the oxidation state of all three materials at the Ni $L_{2,3}$, O K, and Co $L_{2,3}$ edges at five different states of charge. Surface and more bulklike properties are distinguished by total electron yield (TEY) and fluorescence yield (FY) measurements. The electrochemical investigations revealed that the changes in the cell performance of the differently aged materials can be explained by considering the reaction kinetics of the intercalation/deintercalation process. The failure of the redox process of oxygen and nickel at low voltages leads to a significant decrease of the reaction rates in the fatigued cathodes. The accompanied cyclic voltammogram (CV) peaks appear as two peaks because of the local minimum of the reaction rate, although it is one peak in the CV of the calendarically aged LNCAO. The absence of the oxidation/reduction process at low voltages can be traced back to changes in the surface morphology (formation of a NiO-like structure). Further consequences of these material changes are overpotentials, which lead to capacity losses of up to 30% (cycled with a C/3 rate).

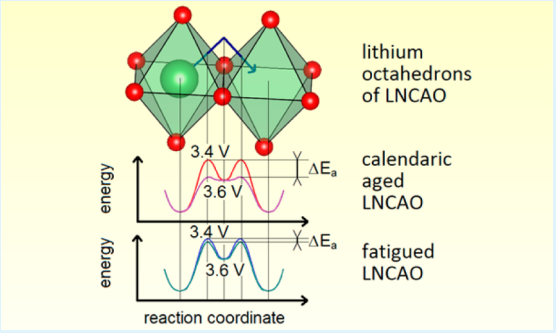

KEYWORDS: *$LiNi_{0.8}Co_{0.15}Al_{0.05}O_2$, degradation mechanism, electronic structure, Ni L, O K, and Co L XAS spectroscopy, GITT*

INTRODUCTION

Lithium ion batteries are commonly used as energy storage devices in many mobile applications such as smart phones and notebooks, due to their high energy and power density. These days, they are also used in electric or hybrid electric vehicles.[1] Therefore, new safety and lifetime requirements have to be fulfilled.

$LiNi_{0.8}Co_{0.15}Al_{0.05}O_2$ (LNCAO) is a commonly used positive electrode material for lithium ion batteries.[2,3] Nevertheless, it shows poor cycling stability at high currents, high temperatures, and large voltage windows.[4] Recently it was shown that capacity losses can be attributed to an incomplete delithiation of LNCAO,[5] which arise due to overpotentials. Overpotentials are reasoned by kinetic limitations. The formation of a NiO-like surface structure, which can cause overpotentials, was reported for LNCAO which was altered at at 60 °C or higher.[6−10] Investigations regarding the relationship between the operation conditions such as the voltage window or the applied current and the fatigue of LNCAO at normal operation conditions of lithium ion batteries (temperatures of 50 °C or lower) are still missing. Furthermore, changes in the intercalation/deintercalation process of LNCAO due to fatigue, as clearly observed by cyclic voltammetry, are hardly understood. As the redox process during charge and discharge of LNCAO is complex and involves partial oxidation of oxygen,[5,9,11,12] its investigation requires the determination of the oxidation state of nickel, cobalt, and oxygen at different states of charge as it was done by Yoon et al. for pristine LNCAO, using X-ray absorption spectroscopy (XAS).[13] Montoro and Rosolen compared Ni $L_{2,3}$ and O K edge spectroscopy results of $LiNi_{0.5}Co_{0.5}O_2$ (isostructural to LNCAO) with diffusion coefficients, determined with the galvanostatic intermittent titration technique

Received: April 14, 2015
Accepted: August 18, 2015
Published: August 18, 2015

DOI: 10.1021/acsami.5b03191
ACS Appl. Mater. Interfaces 2015, 7, 19589−19600

Table 1. Open Cell Voltage (OCV) of the Aged, the Fatigued, and the Highly Fatigued LNCAO versus Lithium after Applying a Relaxation Time of 6 h

	OCV (end of discharge)/V	OCV (end of charge)/V
aged LNCAO vs Li	3.26	4.02
fatigued LNCAO vs Li	3.43	3.98
highly fatigued LNCAO vs Li	3.54	3.91

(GITT), and showed that there is a strong correlation between the reaction rates and the oxygen oxidation/reduction process.[12]

In the present work the correlation between the reaction kinetics and the oxidation/reduction process was investigated for differently charged and aged LNCAO samples. With galvanostatic cycling, cyclic voltammetry, and the galvanostatic intermittent titration technique it is shown that the electrochemical performance of a LNCAO cathode highly depends on the reaction kinetics of the intercalation/deintercalation process. This, in turn, depends on the oxidation/reduction process. The oxidation state of different aged and lithiated LNCAO was investigated with Ni $L_{2,3}$, Co $L_{2,3}$, and O K near-edge X-ray absorption fine structure (NEXAFS) spectroscopy. The measurements were performed in total electron yield (TEY) and fluorescence yield (FY).

The oxidation/reduction of LNCAO proceeds via an electron exchange out of or into the Ni 3d−O 2p band of LNCAO, which was deduced by the modulation of the TEY Ni L edge spectra with multiplet calculations and by the interpretation of the O K spectra in accordance to literature. The FY results are correlated with the changes in the electrochemical behavior observed in cyclic voltammetry (CV), galvanostatic cycling, and GITT experiments. Changes in the surface morphology (formation of a NiO-like surface structure) are resolved by measuring NEXAFS in TEY. The correlation of all results reveals that a hindered nickel and oxygen oxidation/reduction leads to a decrease in the reaction rate and therefore to an increase in the overpotentials at low voltages. At higher voltages, the diffusion of the lithium ions through the altered LNCAO particle surface is hindered.

EXPERIMENTAL SECTION

Samples and Preparation. Two cylindrical JCS 7 Ah lithium ion batteries (detailed information is given in the Supporting Information "Cylindrical 7 Ah lithium ion battery") were cycled for 34 weeks. While keeping the operating temperature at 50 °C and the applied current at 55 A, one cell was cycled between a state of charge (SOC) of 40% and 80% and the other between 79% and 81%. The cells were labeled in accordance with their capacity losses as "highly fatigued" and "fatigued". A calendarically aged cell, stored for 34 weeks at 25 °C (SOC: 30%), was investigated for comparison and labeled as "calendarically aged". More information about the aging process (the durability test) is given in the Supporting Information. For further postmortem investigations (e.g., electrochemical cycling and Ni L XAS measurements) the lithium ion batteries were opened in an argon-filled glovebox. In commercial lithium ion batteries the cathode materials are coated on both sides of an aluminum foil (current collector). For postmortem electrochemical cycling single-side coated electrodes are needed, and therefore, one side of the electrode coating was removed with *N*-methylpyrrolidone. The samples used for further investigations were punched out of the prepared electrodes (12 mm in diameter). The cathode material weighs 4.41 mg cm^{-2} (LNCAO: 80.7 wt %, binder 11.1 wt %, carbon 6.2 wt %).[5]

Electrochemical Measurements. For galvanostatic cycling 24 samples of each 7 Ah JCS cell (eight samples from the outside, the middle, and the inside of the cell package) were mounted in Swagelok cells and cycled 10 times against lithium. Afterward, the mean capacity of the 24 cells with 10 cycles, each, was calculated. The cyclic voltammetry and the galvanostatic intermittent titration technique were performed two times for each 7 Ah JCS cell with samples from the middle of the cell packages. For all electrochemical tests, the LNCAO samples were mounted with Celgard separator, LP30 (organic electrolyte), and lithium as counter and reference electrode in three electrode Swagelok cells. The voltage window for LNCAO versus lithium is 2.8−4.1 V, which was determined previously.[5] The galvanostatic cycles of LNCAO versus lithium were performed with 354 μA cm^{-2} (C/3 rate) and without any holding step. Cyclic voltammetry was done with a sweeping rate of 0.1 V s^{-1}. The galvanostatic intermittent titration technique was performed with a current pulse of 150 μA and a duration of 30 min. The lithium pathway through the LNCAO particles is slightly smaller than the diameter of the particles (around 5 μm). After every pulse a relaxation period of 15 h was given.

BET. The Brunauer−Emmett−Teller (BET) isotherms were measured with a Quantachrome autosorbe iQ system. Before drying the active material at 150 °C under dynamic vacuum for 15 h, the active material was washed with dimethylcarbonate (DMC). The dead volume was reduced with a glass rod.

Cation Separation Process. For an investigation of the LNCAO stoichiometry, the active material was scraped off the current collector and the binder was removed with *N*-methylpyrrolidone (NMP). The remaining material was weighed and put into concentrated hydrochloric acid to dissolve LNCAO. The carbon remained solid and was filtered, washed, dried, and weighed. Cobalt and nickel were precipitated with $(NH_4)_2S$, as is normally done in the cation separation process.[14] The residual material was dissolved in hydrochloric acid again, and cobalt was masked with NH_4SCN and extracted with butanol.[14] Afterward, nickel was precipitated as Ni-$(C_4H_8N_2O_2)_2$.[14] The precipitation reactions were performed four times for 2 mg of the binder-free active material.

XAS Measurements. For the XAS, five LNCAO samples from the middle of the cell packages of the calendarically aged, the fatigued, and the highly fatigued commercial cells were taken. They were cycled three times against lithium with 354 μA cm^{-2} (C/3 rate) to determine the capacity. After galvanostatic cycling the cathodes were discharged to 2.8, 3.4, 3.6, and 3.8 V or charged to 4.1 V, respectively. Afterward, a relaxation time of 6 h was given. The open cell voltage (OCV) depends on the overpotentials and varies for the differently degraded samples. The OCVs at the end of charge and the end of discharge are given in Table 1. The samples were transported to the beamline within an argon-filled transfer case. NEXAFS measurements were carried out at Institute of Solid State Physics's (IFP) soft X-ray beamline WERA at the Karlsruhe synchrotron light source ANKA. The Ni L edge, the O K edge, and the Co L edge were measured with a resolution of 0.2−0.4 eV in TEY and TEY simultaneously. The data analysis included data alignment using a NiO reference, dark current subtraction, division by I_0, and data normalization, described by Reinert et al. previously.[15] The transition metal spectra were calculated with the atomic multiplet and crystal field program CTM4XAS.[16]

RESULTS AND DISCUSSION

1. Electrochemical Characterization. *1.1. Galvanostatic Cycling.* Figure 1 shows galvanostatic cycles of the calendarically aged, the fatigued (cycled between 79% and 81% SOC), and the highly fatigued (cycled between 40% and 80% SOC) positive electrode materials. The fatigued and the highly

DOI: 10.1021/acsami.5b03191
ACS Appl. Mater. Interfaces 2015, 7, 19589−19600

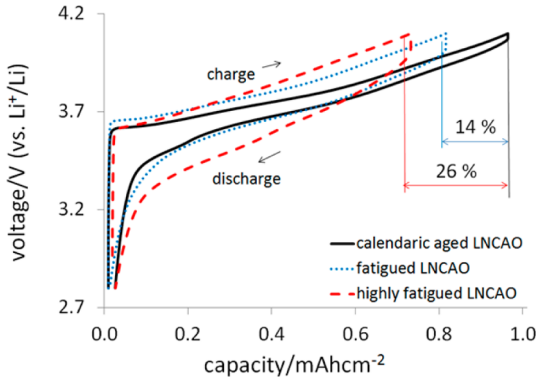

Figure 1. Fifth galvanostatic C/3 cycle of a calendarically aged, a fatigued, and a highly fatigued LNCAO cathode, measured vs lithium. The arrows show the capacity loss of the fatigued cathodes compared to the aged one.

fatigued LNCAO show a capacity loss of 14% ± 5% and 26% ± 9% compared to the calendarically aged material. The losses are the mean values and standard deviations, determined from 24 Swagelok cells and 10 cycles each. Beside the differences in the capacity it is conspicuous that the hysteresis of the fatigued cycles is broader than that of the aged cycles. The width of the cycles at a distinct state of charge (SOC or capacity) is equal to the amount of the overpotentials η in the charge process plus the amount of overpotentials in the discharge process. In comparison with the calendarically aged LNCAO, the overpotentials are almost doubled in the highly fatigued positive material, while they are only slightly higher in the fatigued LNCAO.

1.2. Cylic Voltammetry. Figure 2 shows the cyclic voltammograms (CVs) of the differently degraded positive

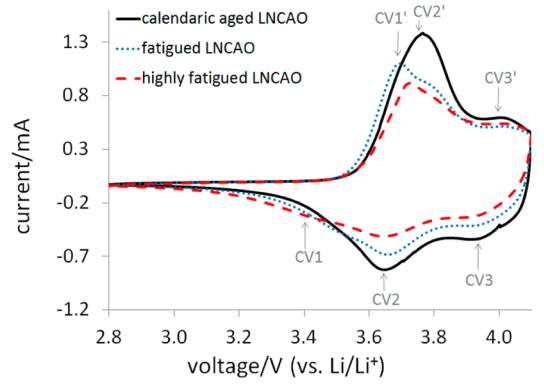

Figure 2. Fifth cyclic voltammogram of the aged, the fatigued, and the highly fatigued LNCAO vs lithium, measured with a sweeping rate of 0.1 V s^{-1}. CV1−CV3 mark the reduction peaks while CV1′−CV3′ mark the oxidation peak in the delithiation/lithiation process of LNCAO.

electrode materials. In the charge and discharge process of the calendarically aged LNCAO only two redox processes (CV2/CV2′ at 3.6 V/3.7 V and CV3/CV3′ at 3.9 V/4.0 V) can be identified. In contrast, the fatigued cathodes show three peaks in the reduction/oxidation process (CV1/CV1′, CV2/CV2′, and CV3/CV3′). The reduction/oxidation peak at 3.6 V/3.7 V of the aged LNCAO is split up into two peaks in the case of the fatigued materials. The different CVs indicate changes in the redox mechanism.

1.3. Galvanostatic Intermittent Titration Technique. A commonly known degradation process in LNCAO is the change of the particle surface morphology at elevated temperatures.[8,9,17,18] An increase in the impedance is associated with these structural changes.[6] It is assumed that the impedance rise is caused by a hindrance of the lithium ion diffusion through the altered surface structure. However, a deeper understanding of the reaction kinetics is still missing. In order to investigate the reaction rate-limiting process, the galvanostatic intermittent titration technique is used. The diffusion coefficient of the rate-limiting reaction step, which is also used in Fick's first law, is called the chemical diffusion coefficient D and can be determined from the galvanostatic intermittent titration (GIT) pulses in accordance to eq 1.

$$D = \frac{4}{\pi t}\left(\frac{\Delta E_s}{\Delta E_t}\right)^2\left(\frac{m_a V_m}{S M_x}\right)^2 \quad (1)$$

ΔE_s describes the difference in the steady-state potentials before and after a current pulse and therefore indicates the changes in potential due to thermodynamics. ΔE_t is the magnitude of the potential changes (without the IR drop) during the current pulse. The time t represents the duration of the current pulse. V_m is the molar volume of LNCAO, determined with Rietveld analysis of XRD patterns of the complete lithiated states. m_a/M_x, the mass divided by the molar mass of LNCAO, gives the quantity of material. The diffusion coefficients are related to the surface collector area S. As to the electrode kinetics in lithium ion batteries, diffusion paths of lithium ions vertical to the current collector surface (in the direction of the electric field) are much faster than horizontal diffusions if a constant current or a constant voltage is applied.[19] Therefore, lithium ions are mostly exchanged between overlaying parts of the electrodes and the reaction rate per surface collector area is the most interesting value.

Figure 3 shows that the chemical diffusion coefficient undergoes changes during charge and discharge of LNCAO.

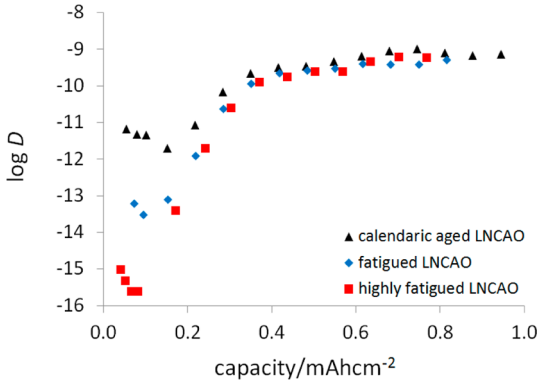

Figure 3. Chemical diffusion coefficient of LNCAO vs lithium as a function of the capacity, determined with GITT.

At 3.5 V, the chemical diffusion coefficient of the fatigued LNCAO is 2 times the logarithm of 10 smaller than that of the calendarically aged sample. In case of the highly fatigued LNCAO, this difference in the diffusion coefficient even amounts to 4 times the logarithm of 10. On the one hand the decrease in the chemical diffusion coefficient per surface collector area could be explained by a decrease of the electrochemically active area, leading to a decreasing reaction

DOI: 10.1021/acsami.5b03191
ACS Appl. Mater. Interfaces 2015, 7, 19589−19600

rate per surface collector. However, the BET surfaces increase from the aged to the highly fatigued samples from 8.6 to 12.5 $m^2\ g^{-1}$. Although the surface areas, measured with BET isotherms, do not show the electrochemically active areas, it is assumed that the electrochemically active areas increase linearly with the BET surface areas. Therefore, the electrochemically active area should also increase and this should lead to higher chemical diffusion coefficients, which, however, is in contrast with the observed behavior. On the other hand the chemical diffusion coefficient can be influenced by overpotentials. With increasing overpotentials, the chemical diffusion coefficient decreases.

In order to investigate the reason for the behavior of the chemical diffusion coefficient, a closer look into the reaction kinetics is necessary. The chemical diffusion coefficient D is a function of the thermodynamic factor Φ and the lithium diffusion coefficient D_{Li+}, eq 2.

$$D = \Phi D_{Li+} \tag{2}$$

The thermodynamic factor comprises the gradient of the steady-state potential E_s of the investigated electrode, which changes during cycling, eq 3.

$$\Phi = \frac{x}{RT}\frac{\Delta E_s}{dx} = \frac{x}{RT}\frac{d(\Delta\mu/zF)}{dx} \tag{3}$$

F is Faraday's constant, x means the Li content in $Li_xNi_{0.8}Co_{0.15}Al_{0.05}O_2$, R is the universal gas constant, T is the absolute temperature in K, and z means the exchanged amount of electrons during oxidation/reduction of one formula unit $Li_xNi_{0.8}Co_{0.15}Al_{0.05}O_2$. Figure 4 shows the steady-state potential,

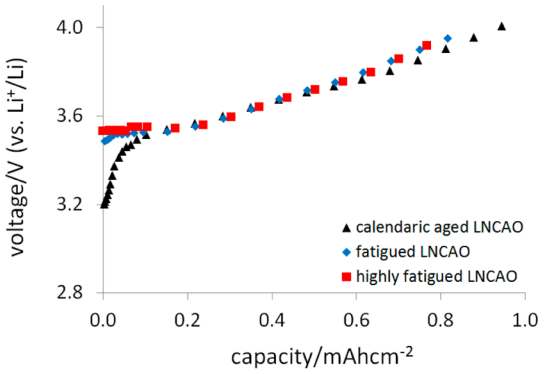

Figure 4. Steady-state potential E_s of LNCAO vs lithium as a function of the capacity, determined with GITT.

which was measured at the end of every relaxation period of the GITT pulses. It should be noted that, in the fully lithiated state of LNCAO, the fatigued cathodes show a different behavior in comparison to the calendarically aged LNCAO. While the steady-state potential of the calendarically aged sample goes down to 3.2 V, the voltage of the fatigued materials stays at around 3.5 V. According to eq 3, the differences in the steady-state potential are also represented in the thermodynamic factor Φ, Figure 5. At around 0.1 mAh cm^{-2}, the fatigued material shows a thermodynamic factor which is 10 times lower and the highly fatigued material shows a thermodynamic factor which is 100 times lower compared to the calendarically aged LNCAO.

In the absence of a gradient the motion of lithium ions at a given temperature is described by the self-diffusion coefficient D_{Li+}. D_{Li+} can be determined by dividing D, the chemical

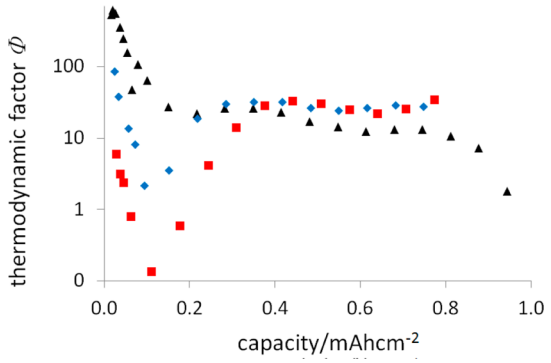

Figure 5. Thermodynamic factor Φ of LNCAO against lithium determined with GITT and plotted as a function of the capacity.

diffusion coefficient, by Φ, the thermodynamic factor eq 2, and it is shown in Figure 6. D_{Li+} of the highly fatigued and

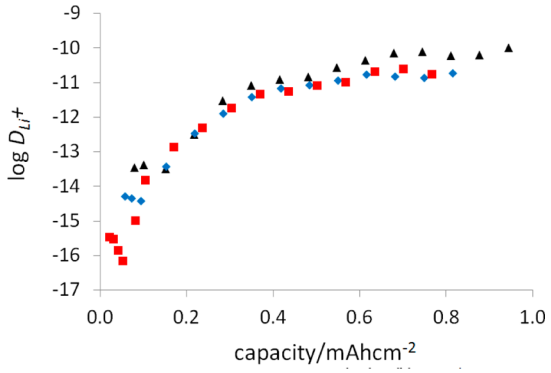

Figure 6. Self-diffusion coefficient D_{Li+} of LNCAO against lithium as a function of the capacity, determined with GITT.

discharged LNCAO is 2 times the power of 10 smaller than that of the calendarically aged material. Slight differences in the self-diffusion coefficient in the order of 10 are observed at high states of charge.

The steady-state potential E_s, which determines the thermodynamic factor, is a function of the difference in the chemical potential $\Delta\mu$ of an electrode and the electrolyte eq 3. If the electric circuit is closed, the difference in the chemical potential between the cathode and the electrolyte or current collector induces the lithium ion and electron transport. The chemical potential, in turn, describes the deviation of the chemical potential of a solid electrode from that of an ideal solution in terms of the logarithm of the activity. The activity is a function of the concentration of mobile lithium ions and mobile electrons within a solid. For this reason, the thermodynamic factor can also be seen as a function of mobile charge carriers within the investigated electrodes.[12,20] The increase of mobile lithium ions results in an increase of the chemical potential. An increasing amount of mobile electrons leads to a decreasing electrochemical potential because the probability of lithium ion recombination increases.[20] This leads to the conclusion that fatigue is caused by a loss of mobile lithium ions or an increase of mobile electrons at low potentials.

1.4. Discussion. The kinetics of the intercalation/deintercalation process has strong influences on the electrochemical performance of a material. In the case of the calendarically aged LNCAO, the thermodynamic factor decreases from the discharged state to 3.5 V and reaches a local maximum at 3.6

DOI: 10.1021/acsami.5b03191
ACS Appl. Mater. Interfaces 2015, 7, 19589−19600

V again. The associated CV (Figure 2, black curve, reduction cycle) shows one peak between 3.4 and 3.8 V (the XAS samples are discharged to a distinct voltage and therefore prepared in the reduction process). In the case of the fatigued materials, the thermodynamic factor decreases faster at low voltages and passes a minimum at 3.5 V, which is up to 100 times lower compared to the thermodynamic factor of the calendarically aged material at this voltage. In addition, the CVs of the fatigued materials show a local minimum at 3.5 V in the reduction process. It may thus be concluded that the slowed down reaction kinetics is the reason for the local minimum in the CVs of the fatigued samples and the peak around 3.6 V appears as two peaks in the fatigued cathodes.

As discussed in the previous sections, the thermodynamic factor Φ depends on the amount of mobile lithium ions within the solid cathode. Below 3.6 V, the devolution of Φ is influenced mainly by two processes: With increasing voltage a lithium concentration gradient is built up, which acts against the applied electric field. That is why surface near regions of the LNCAO particles become lithium ion depleted and the amount of mobile lithium ions initially decreases strongly. At the same time, nickel and oxygen are oxidized. Figure 7 shows that the lithium ions are placed in oxygen octahedra. Due to that, activation energy is necessary to overcome the interactions between lithium and the oxygen shell, if ion motion should take place. The interactions are proportional to the attractive Coulomb interactions (the charge difference between oxygen and lithium), because the lithium−oxygen bond is almost completely ionic in character.[12] With an increasing voltage the charge difference between oxygen and lithium decreases (oxygen is partly oxidized), and therefore, the activation energy for the lithium hopping process decreases.[12] The amount of mobile lithium ions depends in turn on this activation barrier and increases with increasing voltage.

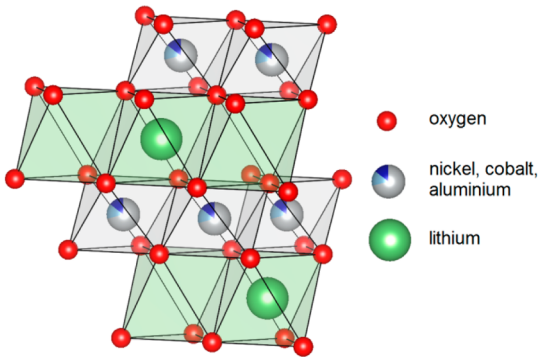

Figure 7. Schematic illustration of the crystal structure of partially delithiated (charged) LNCAO. Nickel, cobalt, aluminum, and lithium are placed in an oxygen octahedron.

Between 3.6 and 3.9 V the thermodynamic factor is almost constant (Figure 5). This constant areas arise from long-range lithium−lithium interactions between different LNCAO layers.[12] Due to these interactions the bond between oxygen and lithium becomes partly covalent in character (attractive interactions between oxygen and lithium), which acts against the decreasing, attractive coulomb interactions.

Above 3.9 V the amount of lithium within LNCAO decreases and becomes reaction rate-limited (up to 3.9 V it was throughput-limited). Parallel to the change from a throughput to a diffusion controlled reaction rate, the interactions between the lithium ions of different layers decreases, which leads to more mobile lithium ions in the LNCAO structure and to a slight increase of the thermodynamic factor at around 3.8 V. This behavior may be the reason for the CV3 peaks in the cyclic voltammograms.

2. Redox Process. *2.1. Oxidation State of Nickel and Oxygen in Discharged LNCAO.* NEXAFS investigations are performed in order to understand the redox process and to investigate the origin of the CV peaks. No phase transition occurs during cycling of LNCAO.[5] This effect was given as explanation of the CV peaks by Sasaki et al.[21] Further studies on the origin of the fine structure of the CVs are missing.

The knowledge of the exact stoichiometry of $LiNi_{0.8}Co_{0.15}Al_{0.05}O_2$ (LNCAO) is necessary to discuss the oxidation states of the transition metals within the material. Small deficiencies or a small excess of either lithium or oxygen would lead to a different formal charge of the transition metals. Inductively coupled plasma optical emission spectroscopy (ICP-OES) results are shown in ref 5 and confirm that the stoichiometric composition of lithium, nickel, cobalt, and aluminum is 1.02(5), 0.80(1), 0.151(3), and 0.048(3), respectively. The further investigation of the cathode material is described in the Experimental Section, "Cation Separation Process". The stoichiometric factor of oxygen was calculated to be 2.04(54). The calculation of the oxygen standard deviation is shown in the Supporting Information. The stoichiometric composition (including the standard deviations) is $Li_{1.02(5)}Ni_{0.80(1)}Co_{0.151(3)}Al_{0.048(3)}O_{2.04(52)}$, and the formal charge of nickel, cobalt, and aluminum is 3+ (lithium, 1+; oxygen, −2). LNCAO crystallizes in the $R\bar{3}m$ space group. The nickel, cobalt, and aluminum atoms occupy the 3a sites while lithium is placed on the 3b sites of the hexagonal setting of the unit cell. All metals are surrounded by six oxygen atoms as shown in Figure 7. Therefore, an octahedral ligand field is assumed for the multiplet calculation of the transition metal spectra. The transition metal spectra were calculated with the software package CTM4XAS.[16]

Figure 8 shows the Ni L edge spectra of the discharged LNCAO, measured in TEY. By measuring in TEY, photo electrons are detected. The emission depth of electrons is around 50 Å. Therefore, this detection mode is surface-sensitive. The peaks in the spectra occur due to Ni 2p → Ni 3d transitions. The shapes of the NEXAFS spectra are related to the electronic ground states of the investigated transition

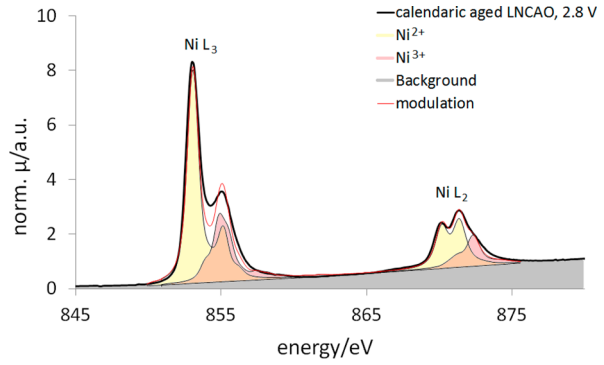

Figure 8. Ni L edge XAS spectrum of calendarically aged, discharged $LiNi_{0.8}Co_{0.15}Al_{0.05}O_2$, measured in TEY. The Ni $L_{2,3}$ spectrum was fitted with a Ni^{2+} and a Ni^{3+} spectrum in an octahedral ligand field, using the software package CTM4XAS (ref 16).

DOI: 10.1021/acsami.5b03191
ACS Appl. Mater. Interfaces 2015, 7, 19589−19600

metals.[22] Although the formal charge of nickel in LNCAO is 3+, the TEY spectra of the discharged LNCAO can only be simulated including a Ni^{2+} and a Ni^{3+} spectrum. The dominant peak at around 853 eV in Figure 8 of the Ni L_3 edge spectrum is typical for Ni^{2+}.[11] The best result for calculating Ni^{2+} and allowing a charge transfer between oxygen and nickel is obtained with around 90% of a d^8 configuration and around 10% of a d^9L configuration, whereby d means the Ni 3d orbitals and L means an electron hole at the oxygen site.[23] The percentages give the electron probability density due to quantum mechanics. The ligand field energy for the 2+ state is approximately 2 eV, which is in agreement with Montoro et al.[22] As to the Ni^{2+} configuration, only the $t^6_{2g}e^2_g$ electronic configuration exists in the ground state because of the Pauli principle and Hund's rule. Due to the presence of Ni^{2+}, an oxygen deficiency should be detected. The formal charge of nickel in defect-free LNCAO is +3 if the oxidation state of oxygen is −2 and the oxidation state of lithium is +1. The presence of Ni^{2+} therefore means that the oxygen stoichiometry should be lower than 2 (the lithium stoichiometry cannot be higher than 1). Due to that the determination of the oxygen stoichiometry is too imprecise. The standard deviation of the oxygen stoichiometry (calculated value: 0.52) was determined using gauss' error propagations. The equations are shown in the Supporting Information. A further method to analyze the oxygen content and to overcome the problems in the future can be high-temperature pyrolysis, wherein a chemical digestion is performed.

The feature around 855 eV in the Ni L_3 edge (Figure 8) can be attributed to a Ni^{3+} state. The simulation revealed that the d^8L configuration with around 60% is preferred over the d^7 configuration (40%). Probably, the Ni^{3+} is stabilized by these charge transfers. Without consideration of the charge transfer of an electron from oxygen toward nickel, additional peaks at higher and lower energies in the L_3 as well as in the L_2 edge of the calculated Ni^{3+} spectrum do not match with the measured data. The determined ligand field energy of Ni^{3+} is around 3 eV. According to the CTM4XAS calculations, Ni^{3+} is a low-spin configuration ($t^6_{2g}e^1_g$).

The modulation shown in Figure 8 is in good agreement with the measured data. All features of the L_3 and the L_2 edge are displayed correctly. Small deviations of the intensity of some peaks can be attributed to inaccuracies in the background correction or to a poor description of the peak broadening.

Figure 9 shows the O K edge of the calendarically aged, discharged LNCAO. Prepeaks at 528.7, 530.5, 531, 532.5, and 535.2 eV (peaks A, B, C, D, and E) are observed. The prepeaks A and B are not present in a NiO spectra (Supporting Information Figure 1). They can be attributed to a Ni^{3+} (d^8L) configuration in accordance to Reinert et al.[15] The peaks C and D look similar to the main peak in the NiO spectra and are attributed to a Ni^{2+} (d^9L) configuration.[15] Differences in the energetic position of the Ni^{2+} LNCAO peak and the NiO peak can be explained by the different band gaps. Peak E at 535.2 eV, next to the absorption edge (535.9 eV), is attributed to transitions into empty molecular orbitals.

Figure 10 shows the Ni L and O K edge, measured in FY. The mean free path length of photons within solids can be 1000 Å. In FY, emitted photons are detected, and therefore, the detection mode is more bulk-sensitive compared to the TEY detection mode. For the evaluation of FY spectra self-absorption and saturation effects have to be considered. Self-absorption occurs due to absorption of photons on their way

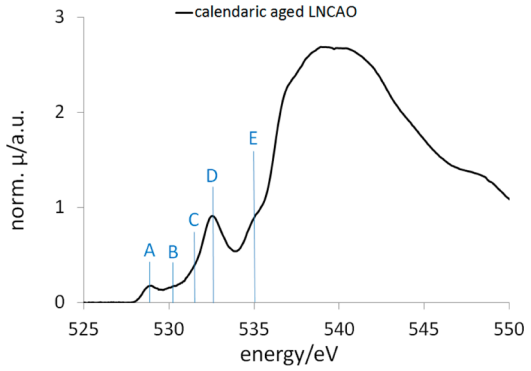

Figure 9. O K edge spectra of fully lithiated (discharged), calendarically aged $LiNi_{0.8}Co_{0.15}Al_{0.05}O_2$. The O K edge shows five prepeaks A–E, while there is only one main prepeak in the NiO spectrum.

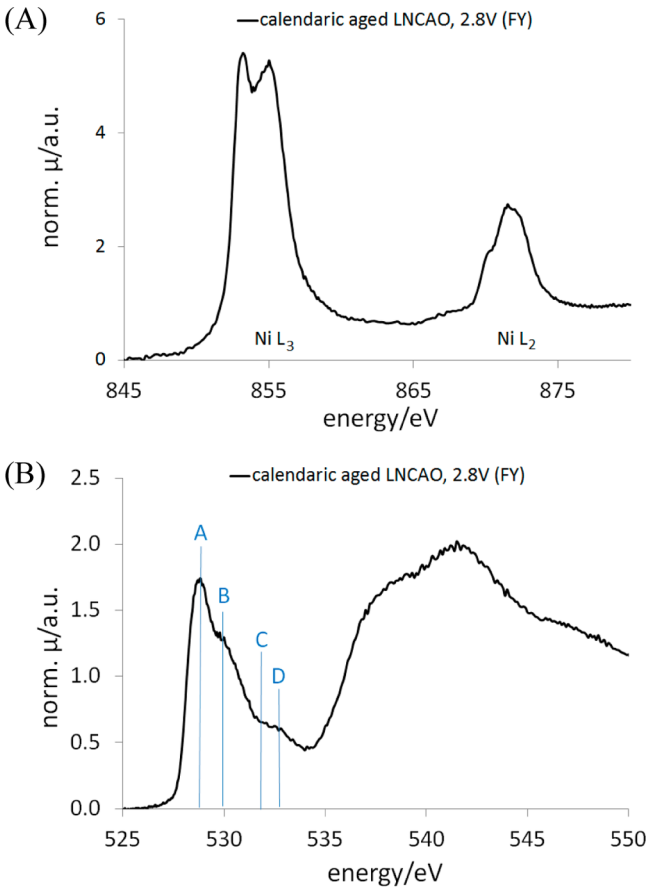

Figure 10. Ni $L_{2,3}$ edge (A) and O K edge XAS spectra (B) of the calendarically aged, discharged LNCAO, measured in FY. The O K FY spectrum shows four pre-edges A–D.

into the sample and absorption of fluorescence radiation on the way out of the sample.[24−26] Saturation effects can change the peak intensity, as well. The main effect of self-absorption and saturation is the depression of peaks with high intensity. Therefore, the ratio of the Ni L_2/Ni L_3 edge is considerably higher using FY measurements than with TEY measurements (Figure 8 and Figure 10A).

As found in Figure 10, parts A and B, the Ni L_3 peak at 855 eV and the peak A in the O K edge spectrum at 528.7 eV are more pronounced compared to the TEY spectra (Figure 8 and

DOI: 10.1021/acsami.5b03191
ACS Appl. Mater. Interfaces 2015, 7, 19589−19600

Figure 9). The former Ni L_3 peak was attributed to Ni^{3+} while the O K prepeak A was attributed to a d^8L configuration (Ni^{3+} with a ligand hole L at the oxygen site). Self-absorption effects may lead to a higher Ni L_3 peak at 853 eV and therefore to a higher Ni^{2+} content. Nevertheless, the L_2 edge is less influenced by self-absorption effects and it shows a main feature around 873 eV, which can be attributed to Ni^{3+} (Figure 10A). As to the TEY spectra, this feature was much lower. In the O K spectra, the first peak at 528.7 eV should be higher due to self-absorption effects. Therefore, the real spectra can be attributed to even higher oxidized LNCAO oxygens, and the Ni^{3+} content is larger in the bulk compared to the surface. Furthermore, a homogeneous distribution of Ni^{2+} and Ni^{3+} within the LNCAO particles can be negated as this would lead to alternating Ni−O distances. With Ni K edge extended X-ray absorption fine structure (EXAFS) analysis it was shown that this is not the case for the investigated LNCAO,[5] although the X-ray absorption process is 10^2 times faster than the electron hopping process, and therefore Ni^{2+} and Ni^{3+} should be distinguishable.[27]

2.2. SOC-Dependent Electronic Structure of the Calendarically Aged LNCAO. The redox processes in positive electrodes take place at the surface/electrolyte interface of the particles.[28−30] Hence, the oxidation/reduction process can be followed by TEY spectra at different states of charge. Figure 11

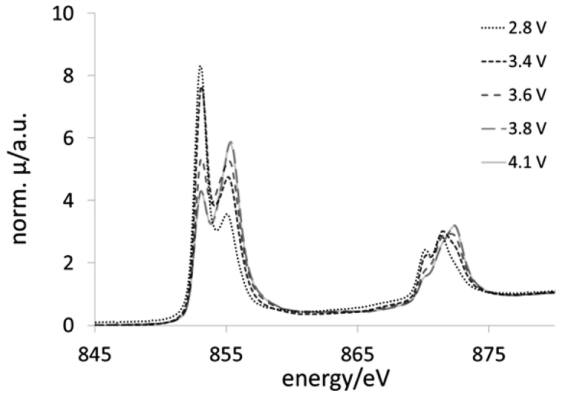

Figure 11. Nickel $L_{2,3}$ edge of calendarically aged LNCAO, discharged to 2.8, 3.4, 3.6, 3.8, and 4.1 V, respectively. The data were measured in TEY mode.

shows the Ni $L_{2,3}$ edge of the calendarically aged LNCAO from 2.8 to 4.1 V. By comparing the measured Ni L edge with the calculated Ni^{2+}/Ni^{3+} spectra (Figure 8) it was deduced that the peak at 853 eV can be attributed to a more Ni^{2+}-like state while the peak at 855 eV can be attributed to a more Ni^{3+}-like state. With an increasing voltage (delithiation of LNCAO) the Ni^{2+} content decreases while the Ni^{3+} content increases. The same observation applies to the L_2 edge. The peaks at 870.1 and 872.6 eV can be attributed to Ni^{2+}. The peak at 872.9 eV is a feature of the Ni^{3+} spectra. While the Ni^{2+} peaks decrease with an increasing voltage, the Ni^{3+} peak increases. In parallel, the O K XAS spectra from 2.8 to 4.1 V exhibit a significant increase of the prepeak at 528.7 eV (Figure 12, peak A). This peak was attributed to a Ni^{3+} (d^8L) configuration. The peak at 532.3 eV (Figure 12, peak B), which was attributed to a Ni^{2+} peak, decreases.

2.3. Redox Behavior of Nickel, Oxygen, and Cobalt. In order to understand the differences in the intercalation/deintercalation process of the fatigued and the calendarically

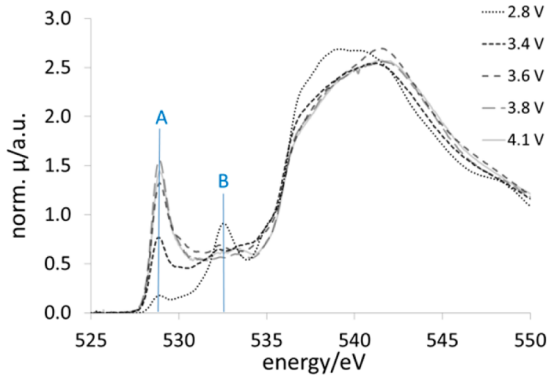

Figure 12. O K edge XAS spectra of the aged LNCAO, discharged to 2.8, 3.4, 3.6, 3.8, and 4.1 V. The data were measured in TEY. The peaks, which mainly change during delithiation are marked with the lines A and B.

aged materials, the different degraded cathodes were investigated with FY XAS measurements at different states of charge. In Figure 13, the Ni L_3, the Ni L_2, and the first prepeaks of the O K edge are shown for the different fatigued cathodes at different SOCs. The Ni^{2+} peaks at 853 eV, 870.1, and 872.6 eV decrease with an increasing voltage while the Ni^{3+} peaks at 855 and 872.9 eV increase (Figure 13, parts A and B). The calendarically aged LNCAO shows changes in the Ni spectra from 2.8 up to 4.1 V, but the changes in the fatigued Ni L spectra between 2.8 and 3.6 V are less obvious. For a better visualization of the changes in the O K spectra, the relative changes in the 528.7 eV FY O K edge peak maxima are shown in Figure 14. In the case of the calendarically aged LNCAO, the peak maximum increases almost continuously (Figure 14). For the highly fatigued LNCAO, the maximum in the O K edge peak intensity remains almost unchanged until 3.6 V. The progression of the O K edge peak maximum of the fatigued material lies between the two cases. The oxygen and the nickel redox process proceeds similarly. This behavior was expected as it was deduced before that the oxidation of nickel and oxygen is highly correlated (the exchanged electrons fill up or leave the Ni 3d−O 2p band). The main difference between the differently aged materials is that the redox process of the fatigued materials takes place at higher voltages than that of calendarically aged LNCAO.

Cobalt (in layered $LiCoO_2$) has a higher redox potential in comparison to nickel (in layered $LiNiO_2$).[31] Therefore, it might be expected that the cobalt oxidation/reduction should take place at potentials higher than 3.8 V (CV3 peak in the cyclic voltammograms) as described by Balasubramanian et al.[32] However, in agreement with other research groups, the Co $L_{2,3}$ spectra almost do not show changes during charge and discharge (Figure 2, Supporting Information).[13,22,31]

2.4. Discussion. During delithiation of LNCAO the Ni−O distance decreases about 0.05 Å, which was determined with powder diffraction and EXAFS analysis.[19] The progression of the Ni−O distance is shown in the Supporting Information Figure 3. The performance of the powder diffraction study and the Ni K XAS (EXAFS) measurements was described elsewhere.[5,19] With Figure 11 and Figure 12 it was shown that the Ni^{3+} content increases during charge and the Ni^{2+} content decreases. This is in agreement with the calculated ligand field energies (2 eV for Ni^{2+} and 3 eV for Ni^{3+}). With an increasing Ni^{3+} content the ligand field gets stronger due to a decreasing distance between oxygen and nickel.

DOI: 10.1021/acsami.5b03191
ACS Appl. Mater. Interfaces 2015, 7, 19589−19600

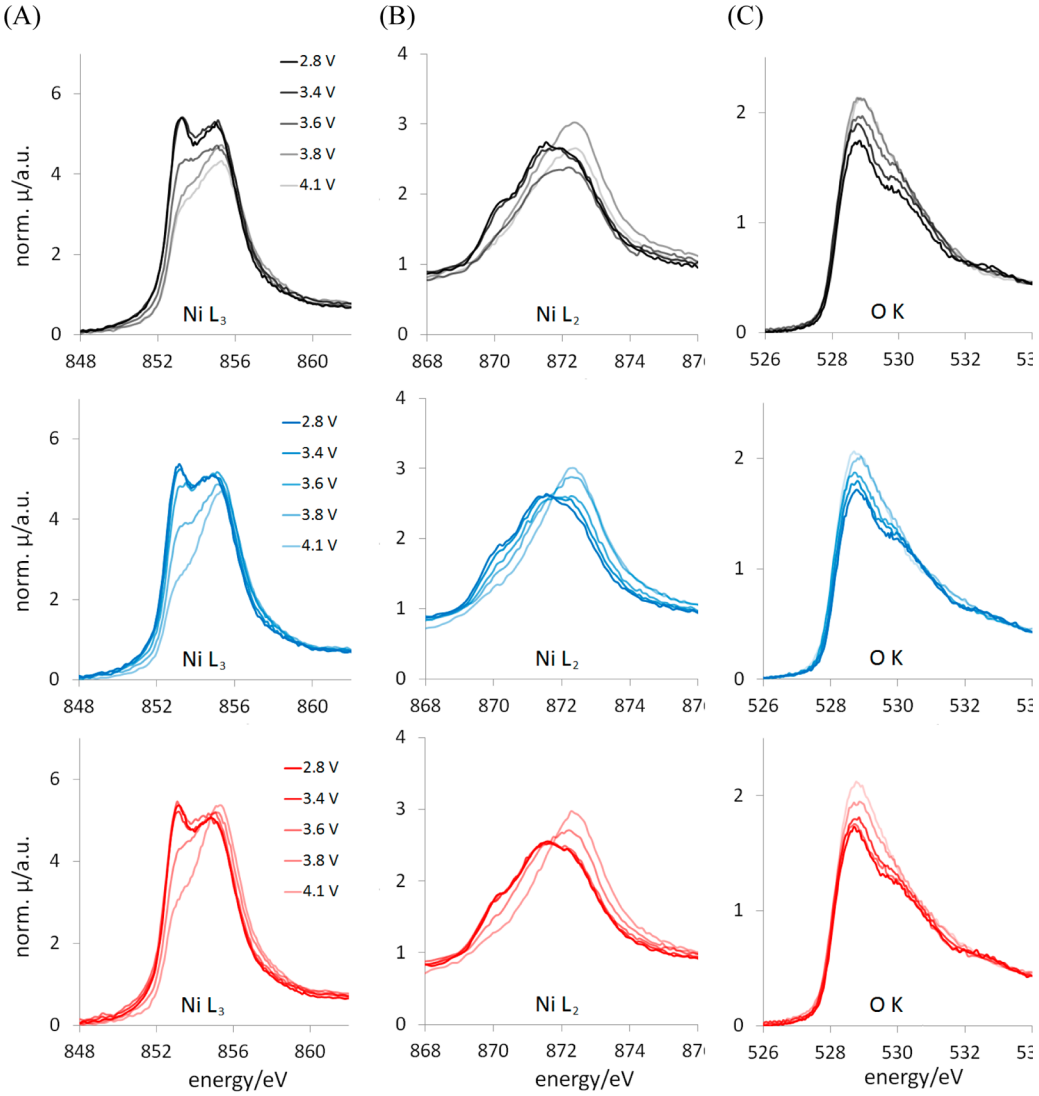

Figure 13. XAS Ni L_3 edge (A), XAS Ni L_2 edge (B), and first prepeaks of the XAS O K edge (C) of the calendarically aged (first row), the fatigued (second row), and the highly fatigued (third row) LNCAO, measured in FY.

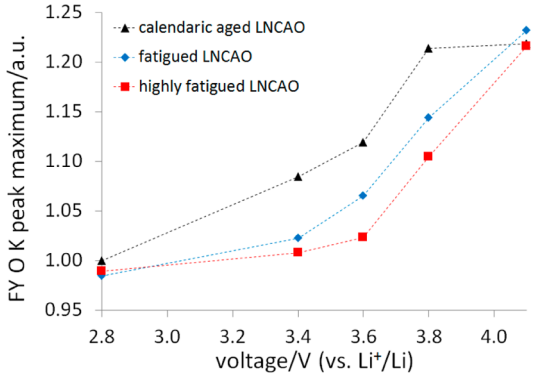

Figure 14. Relative XAS O K peak maximum at 528.7 eV of the calendarically aged, the fatigued, and the highly fatigued LNCAO. The O K peak maximum of the FY spectra was determined relative to the aged 2.8 V sample, which was set to 1.

It was shown that electrons were exchanged from orbitals which have a partially nickel and a partially oxygen character (Ni 3d orbitals hybridized with O 2p orbitals). These orbitals are delocalized over the whole LNCAO structure,[33] which is probably the reason for the high energy density of this kind of material. The exchange of charge is compensated by both the transition metals and the oxygen atoms. But the partial oxidation of oxygen has also a disadvantage. If the oxidation state (the state of delithiation) of LNCAO becomes too high, elemental oxygen can be formed out of the LNCAO structure. This results in a partial oxygen deficit and leads to structural changes as described by Goodenough et al. for $Li_xNi_{1-x}O$ (formation of a NiO-like structure).[34]

As mentioned above, the nickel and the oxygen redox process are closely coupled and cobalt is not oxidized/reduced during lithiation/delithiation of LNCAO. Considering only the redox process of the single elements, only one oxidation/reduction peak should be found in the CVs. However, the calendarically aged LNCAO exhibited two peaks, and three peaks were found for the fatigued cathodes. Hence, the characteristic CVs cannot be explained by considering only the redox process of the elements.

While in the calendarically aged LNCAO both processes start at voltages lower than 3.5 V, the redox process in the fatigued cathodes only takes place at voltages higher than 3.5 V. As discussed in the electrochemistry section, two competitive

DOI: 10.1021/acsami.5b03191
ACS Appl. Mater. Interfaces 2015, 7, 19589−19600

processes determine the reaction kinetics in terms of the thermodynamic factor at 3.5 V. The increasing concentration gradient in the fatigued LNCAO particles leads to a decrease in the thermodynamic factor, and the oxidation of LNCAO (especially of oxygen) leads to a decrease in the activation barrier for lithium motion and therefore to an increase in the thermodynamic factor. However, the redox process, which would lead to an increase in the thermodynamic factor, is hindered in the case of the fatigued material and the thermodynamic factor reaches a minimum at 3.5 V, which is 100 times lower than the thermodynamic factor of the calendarically aged LNCAO.

3. Overpotentials and Capacity Fade. *3.1. Electronic Structure of the Fatigued Cathodes.* Figure 15 shows the TEY

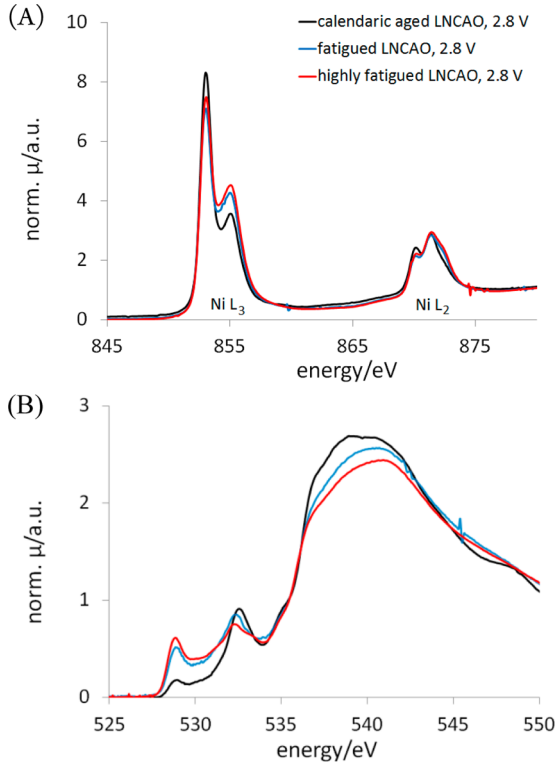

Figure 15. Ni $L_{2,3}$ edge (A) and O K edge (B) of calendarically aged, a fatigued, and a highly fatigued LNCAO in the discharged state. Data were measured in TEY.

XAS spectra of the differently degraded LNCAO cathodes in the discharged state. The second Ni L_3 peak and the first O K prepeak in the fatigued, discharged samples are larger than those of the calendarically aged samples. Figure 11 and Figure 12 show that these peaks significantly increase during delithiation of LNCAO. This reveals that the surfaces of the fatigued LNCAO particles are oxidized more heavily than those of calendarically aged particles, although the lithium content of samples was almost the same (neglecting that lithium can also be present in lithium salts which are formed due to electrolyte decomposition reactions). The results were determined with optical emission spectroscopy (OES) and are shown elsewhere.[5,19] The observation of the more strongly oxidized, fatigued LNCAO particle surfaces is in agreement with the end of discharge voltages of the differently degraded cathodes (Table 1), which are around 0.1 V higher than the OCV of the calendarically aged sample.

3.2. NiO-Like Surface Structure. A detailed investigation of the TEY O K edge spectra around 533 eV (Figure 16A) shows even more differences between the differently degraded cells. The Ni^{2+} features, discussed and displayed in the section "Oxidation State of Nickel and Oxygen in Discharged LNCAO", are more shifted to lower energies the more the samples are degraded. In accordance to Mori et al, this can be attributed to the formation of a NiO-like structure.[8] As can be seen in the NiO reference spectrum above the LNCAO spectra (Figure 16A), the NiO peaks are about 0.5 eV lower than the Ni^{2+} features of the calendarically aged LNCAO. Furthermore, the Ni^{2+} peaks decrease in the calendarically aged cathode from 2.8 to 4.1 V, while they are still present at 4.1 V in the fatigued materials.

In a NiO-like structure, which is built out of the rhombohedral LNCAO structure, some nickel atoms occupy lithium sites and the structure becomes monoclinic distorted. Goodenough showed that $Li_xNi_{1-x}O$ ($Li_{x/(1-x)}NiO_{1/(1-x)}$, which is isostructural to LNCAO for $x > 0.6$) changes its structure from rhombohedral to cubic (more accurate, monoclinic distorted) when x gets lower than 0.6.[34] This effect is connected with oxygen losses in the crystal structure.[18,35] The fully delithiated state of $Li_xNi_{1-x}O$ is the monoclinic distorted NiO. Although $Li_xNi_{0.8}Co_{0.15}Al_{0.05}O_2$ (LNCAO) is isostructural to Li_xNiO_2 ($Li_{x/(1-x)}NiO_{1/(1-x)}$, x = 0.5) and has a similar composition, it shows a better cycling stability.[36−38] Nevertheless, it was found that oxygen loss takes place in LNCAO at lithium contents x lower than 0.4.[18,35] This can also lead to a NiO-like structure.

3.3. Discussion. Even in the delithiated (charged) state of LNCAO (4.1 V vs lithium), the mean lithium content is higher than 0.4.[5,19] Furthermore, only the surfaces of the LNCAO particles show a NiO-like structure, which can be seen by comparing the O K TEY measurements at around 533 eV with the O K FY measurements in the same energy region, Figure 16, parts A and B. No peak shift was found in the more bulk-sensitive FY measurements, and the SOC-dependent spectra of the fatigued materials do not differ significantly from the spectra of the calendarically aged LNCAO. The aspects mentioned above might lead to the conclusion that only a lithium gradient within the LNCAO particles can cause lithium contents x in $Li_xNi_{0.8}Co_{0.15}Al_{0.05}O_2$ lower than 0.4 in surface near regions. The fatigued material was cycled with a current of 55 A (nearly an 8C-rate) between 79% and 81% SOC in the durability test. The highly fatigued LNCAO was cycled with the same C-rate between 40% and 80% SOC. The lithium gradient inside the LNCAO particles is therefore lower in the fatigued material at the end of every charging process, because the charging time is shorter. In agreement with that the observed degradations of the fatigued LNCAO particles are less pronounced.

The OCV of a cell depends on the temperatures. At higher temperatures the OCV is lower although the lithium content is the same. Due to that, the material is stronger delithiated while applying the end of charge voltage at higher temperatures. This has the same effect as a cycling gradient in surface near regions of the material and leads to the same degradations. Nevertheless, a careful analysis of the fluorescence and TEY spectra of different SOCs and temperatures between 530 and 538 eV is still missing. For that reason the question whether only the surface or both surface and bulk are influenced by temperature degradations is still open.

DOI: 10.1021/acsami.5b03191
ACS Appl. Mater. Interfaces 2015, 7, 19589−19600

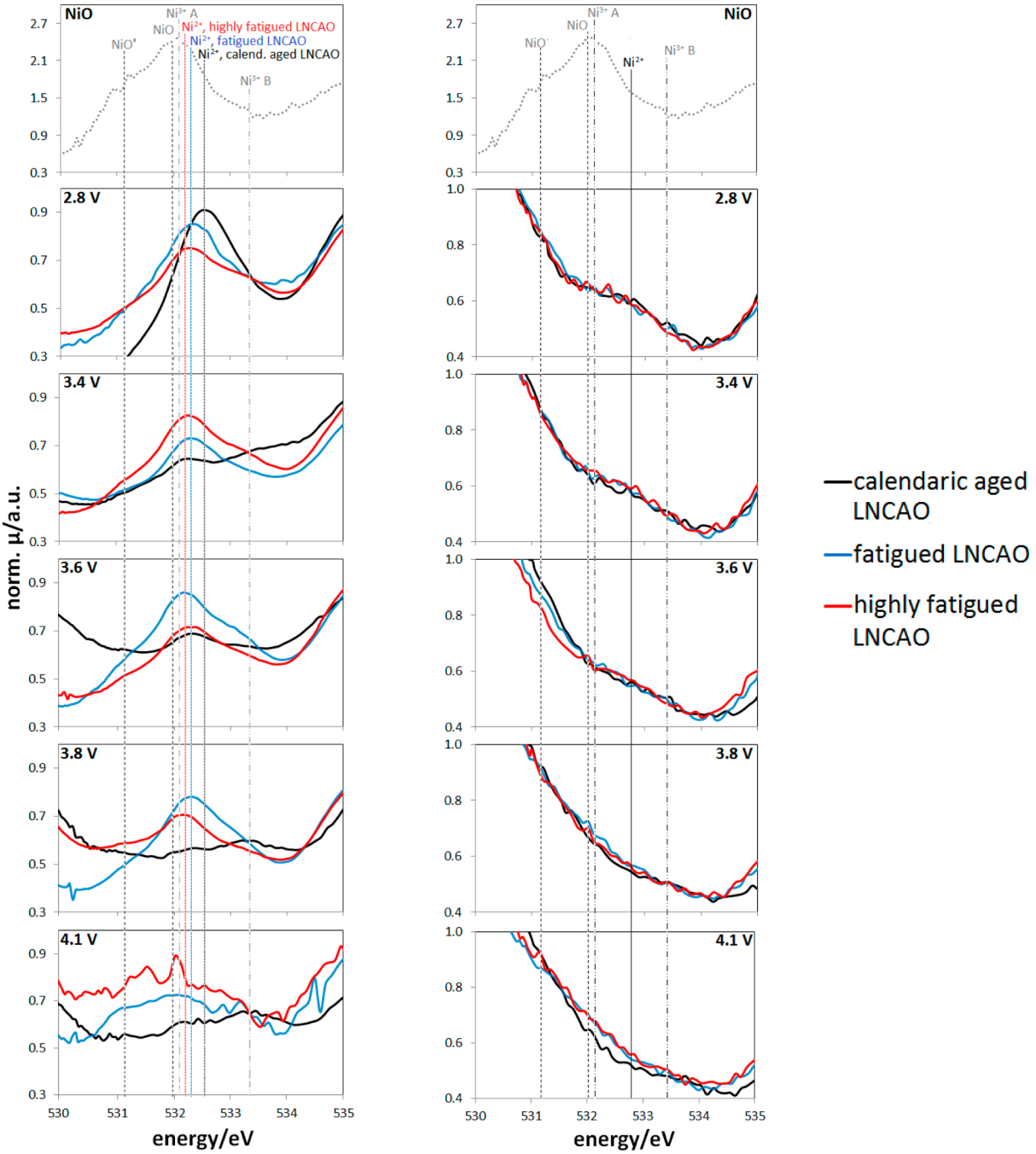

Figure 16. O K edge spectra from 530 to 535 eV of the aged (black curves), the fatigued (blue curves), and the highly fatigued LNCAO (red curves), measured in TEY (A) and FY (B). Above the different spectra of the different SOCs a spectra of a NiO reference is shown.

The fully lithiated state of a NiO-like structure can hardly be achieved, and the OCV at the end of discharge does not reach the OCV of the calendarically aged sample in the discharged state, which was shown in Table 1. Furthermore, the changes of the surface morphology lead to overpotentials, because randomly distributed nickel atoms (nickel occupies also lithium sites in a NiO-like structure) block the lithium diffusion pathways. The overpotentials increase with increasing fatigue, Figure 1.

The capacity of LNCAO highly depends on the applied current density of the galvanostatic cycles.[5,19] With a decreasing C-rate the capacity loss converges against zero. This suggests that all observed capacity losses are due to kinetic problems (overpotentials). The broadening of the galvanostatic cycling curves shows that the overpotentials increase from the calendarically aged over the fatigued to the highly fatigued samples, which explains the increase of the capacity losses.

The higher overpotentials lead to higher OCVs at the end of discharge and to lower OCVs at the end of charge, Table 1. It also reveals that the fatigued materials cannot be fully charged by applying a constant current. Powder diffraction and EXAFS analysis show that completely lithiated domains exist in the highly fatigued materials, even at the end of charge voltage of 4.1 V against lithium.[5] The presence of fully lithiated LNCAO domains was observed above 3.6 V (LNCAO vs lithium) for all cathodes.[5] Below this voltage it was not possible to distinguish

DOI: 10.1021/acsami.5b03191
ACS Appl. Mater. Interfaces 2015, 7, 19589−19600

between fully lithiated and partially delithiated domains. The volume fractions of these domains decrease with an increasing voltage.[5] Therefore, it is assumed that the LNCAO particles are delithiated from the outside toward the inside. The lithiated domains vanish at 3.8 V in the calendarically aged sample. In contrast, fully lithiated domains are still present in the fatigued samples at 4.1 V. Table 2 lists the measured capacity losses and

Table 2. Mean Capacity Loss of 24 LNCAO Samples versus Lithium (10 Cycles Each) for Two Differently Fatigued Positive Electrode Materials and the Electrochemically Inactive LNCAO Phase Content, Determined with Powder Diffraction[a,b]

	capacity loss/%	inactive phase/%
aged LNCAO vs Li	0 ± 2	
fatigued LNCAO vs Li	14 ± 5	10
highly fatigued LNCAO vs Li	26 ± 9	29

[a]Refs 5 and 19. [b]The results were determined relative to the capacity of calendarically aged LNCAO.

the phase contents of the fully lithiated LNCAO domains at the end of charge. The detailed electrochemical EXAFS and powder diffraction results were shown elsewhere.[5,19] The incomplete delithiation of the charged cathodes lead to the observed capacity losses.

In order to improve the materials in the future, the surfaces of the particles can be modified. It is imaginable to replace oxygen in the outer parts of the LNCAO particles with fluorine, because fluorine can hardly be oxidized and therefore no anion deficit occurs. This structure should then be more stable. But fluorine does not form delocalized, molecular orbitals (like Ni d−O 2p orbitals do), and therefore, the electron exchange can only take place at the transition metal sites.

CONCLUSION

LNCAO shows capacity losses up to 30% under distinct durability conditions and a change in the intercalation/deintercalation process as found with cyclic voltammetry. The intercalation/deintercalation process depends on the kinetics of the diffusion processes within the materials, and the oxidation/reduction of the transition metals or oxygen plays only a secondary role. The CVs show a strong correlation with changes in the diffusion coefficients, determined with GITT. In the calendarically aged electrode, the redox process starts at the end of discharge voltage and the charge difference between oxygen and lithium becomes lower with increasing delithiation. In contrast, the redox process of the fatigued cathodes is hindered at low states of charge and the effective charge of oxygen stays constant. The charge difference between oxygen and lithium determines, among others, the activation barrier for the lithium diffusion process within LNCAO (lithium is placed in an oxygen octahedron). Therefore, the activation barrier for the lithium diffusion process does not decrease in the fatigued samples at low states of charge. This leads to lower chemical potentials at the same applied potential. Hence, an increase in the overpotentials is observed with increasing fatigue. The differences in the redox behavior and the increase in the overpotentials arise from the formation of a NiO-like surface structure. The overpotentials lead to an incomplete delithiation of LNCAO and therefore to a decreasing capacity. Moreover, it was discussed that during cycling a lithium gradient within the LNCAO particles can be the origin of the degradations. This lithium gradient increases with increasing currents and a larger voltage window, in which the cathodes are cycled.

ASSOCIATED CONTENT

Supporting Information

The Supporting Information is available free of charge on the ACS Publications website at DOI: 10.1021/acsami.5b03191.

Cell parameters of the investigated 7 Ah JCS cells, description of the performed durability test, determination of the standard deviation of the oxygen stoichiometry, an O K reference spectrum of NiO, FY Co $L_{2/3}$ XAS spectra of the different aged cathodes at different states of charge, Ni−O bond distances in LNCAO determined with powder diffraction and EXAFS analysis (PDF)

AUTHOR INFORMATION

Corresponding Author

*E-mail: karin.kleiner@kit.edu.

Notes

The authors declare no competing financial interest.

ACKNOWLEDGMENTS

We acknowledge the Synchrotron Light Source ANKA for provision of beamtime. Further, we acknowledge Dominik Haering for the BET measurements and Christina Roth for proofreading. The work was funded by the BMW group. A part of this work was supported by the Helmholtz Association via the programs STN, NANOMICRO, KNMF, PNI, and MML.

REFERENCES

(1) Andre, D.; Kim, S.-J.; Lamp, P.; Lux, S. F.; Maglia, F.; Paschos, O.; Stiaszny, B. Future Generations of Cathode Materials: An Automotive Industry Perspective. *J. Mater. Chem. A* **2015**, *3*, 6709−6732.

(2) Etacheri, V.; Marom, R.; Elazari, R.; Salitra, G.; Aurbach, D. Challenges in the Development of Advanced Li-Ion Batteries: A Review. *Energy Environ. Sci.* **2011**, *4* (9), 3243.

(3) Thielmann, A.; Isenmann, R.; Wietdchel, M. *Technology-Roadmap Lithium-Ion-Batteries 2030*; Fraunhofer ISI: Karlsruhe, Germany, 2010.

(4) Haering, D. Investigation of Aging Effects on Lithium-Ion Cells with Electric Measuring Techniques. Technische Universität München, Ph.D. Thesis, 2012.

(5) Kleiner, K.; Dixon, D.; Jakes, P.; Melke, J.; Yavuz, M.; Roth, C.; Nikolowski, K.; Liebau, V.; Ehrenberg, H. Fatigue of LiNi0.8Co0.15Al0.05O2 in Commercial Li Ion Batteries. *J. Power Sources* **2015**, *273*, 70−82.

(6) Kojima, Y.; Muto, S.; Tatsumi, K.; Kondo, H.; Oka, H.; Horibuchi, K.; Ukyo, Y. Degradation Analysis of a Ni-Based Layered Positive-Electrode Active Material Cycled at Elevated Temperatures Studied by Scanning Transmission Electron Microscopy and Electron Energy-Loss Spectroscopy. *J. Power Sources* **2011**, *196* (18), 7721−7727.

(7) Avendaño, E.; Rensmo, H.; Azens, a.; Sandell, a.; Azevedo, G. D. M.; Siegbahn, H.; Niklasson, G. a.; Granqvist, C. G. Coloration Mechanism in Proton-Intercalated Electrochromic Hydrated NiO[sub Y] and Ni[sub 1−x]V[sub x]O[sub Y] Thin Films. *J. Electrochem. Soc.* **2009**, *156* (8), P132.

(8) Mori, D.; Kobayashi, H.; Shikano, M.; Nitani, H.; Kageyama, H.; Koike, S.; Sakaebe, H.; Tatsumi, K. Bulk and Surface Structure Investigation for the Positive Electrodes of Degraded Lithium-Ion Cell after Storage Test Using X-Ray Absorption near-Edge Structure Measurement. *J. Power Sources* **2009**, *189* (1), 676−680.

DOI: 10.1021/acsami.5b03191
ACS Appl. Mater. Interfaces 2015, 7, 19589−19600

(9) Muto, S.; Sasano, Y.; Tatsumi, K.; Sasaki, T.; Horibuchi, K.; Takeuchi, Y.; Ukyo, Y. Capacity-Fading Mechanisms of LiNiO[sub 2]-Based Lithium-Ion Batteries. *J. Electrochem. Soc.* **2009**, *156* (5), A371.
(10) Nonaka, T.; Okuda, C.; Seno, Y.; Koumoto, K.; Ukyo, Y. X-Ray Absorption Study on LiNi0.8Co0.15Al0.05O2 Cathode Material for Lithium-Ion Batteries. *Ceram. Int.* **2008**, *34* (4), 859−862.
(11) Kobayashi, H.; Shikano, M.; Koike, S.; Sakaebe, H.; Tatsumi, K. Investigation of Positive Electrodes after Cycle Testing of High-Power Li-Ion Battery Cells. *J. Power Sources* **2007**, *174* (2), 380−386.
(12) Montoro, L. A.; Rosolen, J. M. The Role of Structural and Electronic Alterations on the Lithium Diffusion in LixCo0.5Ni0.5O2. *Electrochim. Acta* **2004**, *49* (19), 3243−3249.
(13) Yoon, W.-S.; Chung, K. Y.; McBreen, J.; Fischer, D. a.; Yang, X.-Q. Electronic Structural Changes of the Electrochemically Li-Ion Deintercalated LiNi0.8Co0.15Al0.05O2 Cathode Material Investigated by X-Ray Absorption Spectroscopy. *J. Power Sources* **2007**, *174* (2), 1015−1020.
(14) Strähle, J.; Schweda, E. *Jander Blasius, Textbook of Analytical and Preparative Inorganic Chemistry*, 16th ed.; S. Hirzel Verlag: Stuttgart, Germany, 2006; p 728.
(15) Reinert, F.; Steiner, P.; Hüfner, S.; Schmitt, H.; Fink, J.; Knupfer, M.; Sandl, P.; Bertel, E. Electron and Hole Doping in NiO. *Z. Phys. B: Condens. Matter* **1995**, *97*, 83−93.
(16) Ikeno, H.; de Groot, F. M. F.; Stavitski, E.; Tanaka, I. Multiplet Calculations of L(2,3) X-Ray Absorption near-Edge Structures for 3d Transition-Metal Compounds. *J. Phys.: Condens. Matter* **2009**, *21* (10), 104208.
(17) Watanabe, S.; Kinoshita, M.; Hosokawa, T.; Morigaki, K.; Nakura, K. Capacity Fade of LiAlyNi1−x−yCoxO2 Cathode for Lithium-Ion Batteries during Accelerated Calendar and Cycle Life Tests (surface Analysis of LiAlyNi1−x−yCoxO2 Cathode after Cycle Tests in Restricted Depth of Discharge Ranges). *J. Power Sources* **2014**, *258*, 210−217.
(18) Hwang, S.; Kim, S. M.; Bak, S.-M.; Cho, B.-W.; Chung, K. Y.; Lee, J. Y.; Chang, W.; Stach, E. A. Investigating Local Degradation and Thermal Stability of Charged Nickel-Based Cathode Materials through Real-Time Electron Microscopy. *ACS Appl. Mater. Interfaces* **2014**, *6*, 15140−15147.
(19) Kleiner, K. Chemical Investigation of Aging Mechanisms in Lithium-Ion Batteries. Ph.D. Thesis, Institute for Applied Materials−Energy Storage Systems, Karlsruhe Institute of Technology, Karlsruhe, Germany, 2014.
(20) Weppner, W.; Huggins, R. a. Electrochemical Methods for Determining Kinetic Properties of Solids. *Annu. Rev. Mater. Sci.* **1978**, *8* (1), 269−311.
(21) Sasaki, T.; Nonaka, T.; Oka, H.; Okuda, C.; Itou, Y.; Kondo, Y.; Takeuchi, Y.; Ukyo, Y.; Tatsumi, K.; Muto, S. Capacity-Fading Mechanisms of LiNiO2-Based Lithium-Ion Batteries. *J. Electrochem. Soc.* **2009**, *156*, A289−A293.
(22) Montoro, L. A.; Abbate, M.; Rosolen, J. M. Electronic Structure of Transition Metal Ions in Deintercalated and Reintercalated LiCo[sub 0.5]Ni[sub 0.5]O[sub 2]. *J. Electrochem. Soc.* **2000**, *147* (5), 1651−1657.
(23) Van Elp, J.; Searle, B. G.; Sawatzky, G. A.; Sacchi, M. Ligand Hole Induced Symmetry Mixing of d8 States in LixNi1−xO, as Observed in Ni 2p X-Ray Absorption Spectroscopy. *Solid State Commun.* **1991**, *80* (1), 67−71.
(24) Jaklevic, J.; Kirby, J. A.; Klein, M. P.; Robertson, A. S.; Brown, G. S.; Eisenberger, P. Fluorescence Detection of EXAFS: Sensitivity Enhancement for Dilute Species and Thin Films. *Solid State Commun.* **1993**, *88*, 1105−1108.
(25) Eisebitt, S.; Böske, T.; Rubensson, J. E.; Eberhardt, W. Determination of Absorption Coefficients for Concentrated Samples by Fluorescence Detection. *Phys. Rev. B: Condens. Matter Mater. Phys.* **1993**, *47*, 14103−14109.
(26) Tröger, L.; Arvanitis, D.; Baberschke, K.; Michaelis, H.; Grimm, U.; Zschech, E. Full Correction of the Self-Absorption in Soft-Fluorescence Extended X-Ray-Absorption Fine Structure. *Phys. Rev. B: Condens. Matter Mater. Phys.* **1992**, *46*, 3283−3289.
(27) Bisquert, J. Chemical Diffusion Coefficient of Electrons in Nanostructured Semiconductor Electrodes and Dye-Sensitized Solar Cells. *J. Phys. Chem. B* **2004**, *108*, 2323−2332.
(28) Brenet, J. P. The Charge Transfer Od Electrochemical Generators. *Electrochim. Acta* **1964**, *9*, 659−665.
(29) Gerischer, H. Electron-Transfer Kinetics of Redox Reactions at the Semiconductor/Electrolyte Contact. A New Approach. *J. Phys. Chem.* **1991**, *95* (3), 1356−1359.
(30) Jamnik, J. Charge Transport and Chemical Diffusion Involving Boundaries. *Solid State Ionics* **1997**, *94* (1−4), 189−198.
(31) Ohzuku, T.; Makimura, Y. Formation of Solid Solution and Its Effect on Lithium Insertion Schemes for Advanced Lithium-Ion Batteries: X-Ray Absorption Spectroscopy and X-Ray Diffraction of LiCoO2, LiCo1/2Ni1/2O2 and LiNiO2. *Res. Chem. Intermed.* **2006**, *32* (5), 507−521.
(32) Balasubramanian, M.; Sun, X.; Yang, X. Q.; Mcbreen, J. In Situ X-Ray Absorption Studies of a High-Rate LiNi 0. 85 Co 0. 15 O 2 Cathode Material. *J. Electrochem. Soc.* **2000**, *147* (8), 2903−2909.
(33) Laubach, S.; Laubach, S.; Schmidt, P. C.; Ensling, D.; Schmid, S.; Jaegermann, W.; Thissen, A.; Nikolowski, K.; Ehrenberg, H. Changes in the Crystal and Electronic Structure of LiCoO(2) and LiNiO(2) upon Li Intercalation and de-Intercalation. *Phys. Chem. Chem. Phys.* **2009**, *11* (17), 3278−3289.
(34) Goodenough, J. B.; Wickham, D. G.; Croft, W. J. Some Magnetic and Crystallographic Properties of the System LixNi1-xO. *J. Phys. Chem. Solids* **1958**, *5*, 107−116.
(35) Bak, S.; Nam, K.; Chang, W.; Yu, X.; Hu, E.; Hwang, S.; Stach, E. A.; Kim, K.-B.; Chung, K. Y.; Yang, X.-Q. Correlating Structural Changes and Gas Evolution during the Thermal Decomposition of Charged Li X Ni 0.8 Co 0.15 Al 0.05 O 2 Cathode Materials. *Chem. Mater.* **2013**, *25* (3), 337−351.
(36) Cao, H.; Xia, B.; Xu, N.; Zhang, C. Structural and Electrochemical Characteristics of Co and Al Co-Doped Lithium Nickelate Cathode Materials for Lithium-Ion Batteries. *J. Alloys Compd.* **2004**, *376* (1−2), 282−286.
(37) Han, C. J.; Yoon, J. H.; Cho, W.; Jang, H. Electrochemical Properties of LiNi0.8Co0.2−xAlxO2 Prepared by a Sol−gel Method. *J. Power Sources* **2004**, *136* (1), 132−138.
(38) Kalyani, P.; Kalaiselvi, N.; Renganathan, N. G.; Raghavan, M. Studies on LiNi0.7Al0.3−xCoxO2 Solid Solutions as Alternative Cathode Materials for Lithium Batteries. *Mater. Res. Bull.* **2004**, *39* (1), 41−54.

DOI: 10.1021/acsami.5b03191
ACS Appl. Mater. Interfaces 2015, 7, 19589−19600